GeoStudio Example File
Convection cells in groundwater

To see the latest GeoStudio learning content, visit Seequent Learning Centre and search the catalogue for “GeoStudio”.

Introduction

Yang et al. (2010) studied the effect of topography driven flow on the development of convection cells in a groundwater aquifer. Topography driven flow refers to cases where elevation differences result in a sloping groundwater table. Temperature differences can result in buoyancy driven convective groundwater flow.

The objective here is to replicate some of the analyses presented by Yang et al. (2010) in an effort to determine if GeoStudio is suitable for these types of analyses.

Background

Yang et al. (2010) looked at the importance of the topography driven flow relative to the buoyancy driven flow. They discovered the presence of four convective cells in their base case as illustrated in Figure 1. They used a sand aquifer 200 m deep and 800 m long with the groundwater table at the surface.

Free convection cells can only form under certain conditions. The buoyancy forces arising from temperature differences need to be significantly higher than the diffusive forces. The ratio of these two forces is defined by what is known as the Raleigh number.

For a porous medium, the Rayleigh number (N_{RA}) is defined as:

$$N_{RA} = \frac{g\Delta\rho H}{D\mu}k$$

Equation 1

where g is the gravitation constant (9.807 m/s²), $\Delta\rho$ is the range in densities (1.44 kg/m³), H is the distance top to bottom (200 m), D is the diffusivity (m²/s), μ is the dynamic viscosity (1.787x10^{-3} kg/m/s) and k is the intrinsic permeability (m²) (Lapwood, 1948).

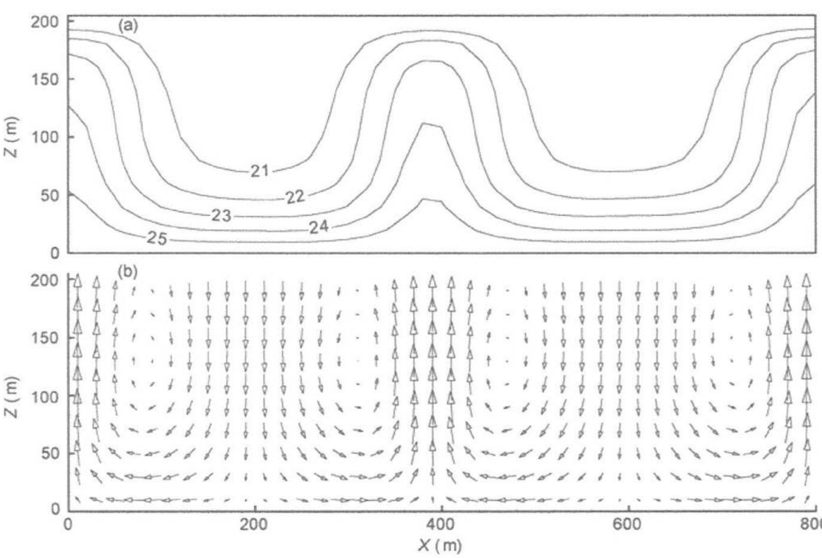

Figure 1. Temperature contours and flow vectors for the case of perfectly flat ground as presented by Yang et al. (2010).

The diffusivity (D) is defined as:

$$D = \frac{K_t}{c_w \rho_0} = \frac{2.18}{4174 \times 1000} = 5.22 \times 10^{-7}\, m^2/sec$$

Equation 2

where K_t is the thermal conductivity for the soil-water matrix (J/sec/m/°C), c_w is the specific heat capacity of the water (J/kg/°C) and ρ_0 is the density of the water (1000 kg/m^3). Substituting these values into the N_{RA} equation gives,

$$N_{RA} = \frac{g\ \Delta\rho\ H}{D\ \mu} k = \frac{9.801\ \times\ (998.21 - 996.77)\ \times\ 200}{5.22x10^{-7}\ \times\ 1.787x10^{-3}} k = 3.03 \times 10^{12} k$$

Equation 3

Yang et al. (2010) report the intrinsic permeability as 10^{-11} m^2. This results in the N_{RA} being equal to 30.6. This is slightly different than the N_{RA} value of 35 given in the paper. The paper does not indicate the exact values used to calculate N_{RA}. Regardless, the values are reasonably close.

A N_{RA} value in the 30's is at the low end of what is required to imitate the on-set of free convection. Holzbecher (1998) suggests the value should be at least 40. This seems consistent with observations made during the numerical experimentation here. It was not possible to imitate the free convention with the above computed N_{RA} value of the 30.6

Various higher N_{RA} values were consequently tried. Ultimately, an N_{RA} value of 67 was selected for the analyses here. This value was elected to give a reasonable hydraulic conductivity as presented in the next section.

Numerical Simulation

The model domain was developed using the same dimensions given by Yang et al. (2010), as shown in Figure 2. An attempt was made here to use the material properties presented in the Yang et al. (2010) paper, but this was only partially successful. There are some typographical errors and it is not entirely clear how some values were determined. Nonetheless, the data presented in the paper are sufficient for the example objectives.

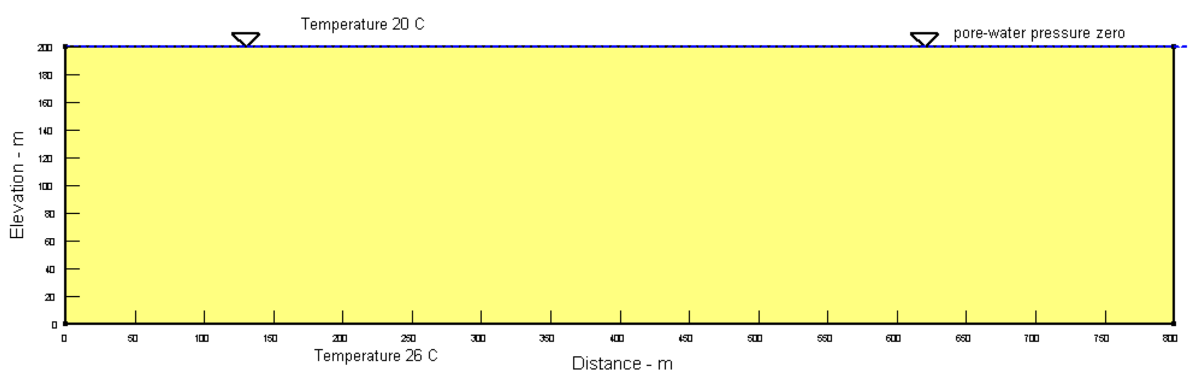

Figure 2. Problem configuration.

This is fundamentally a water transfer problem, so a transient SEEP/W analysis was used. The Heat transfer option was included in the analysis, with both the thermal free convection and forced convection with water transfer options turned on in the Physics tab (Figure 3). The initial pore-water pressure conditions were defined using a water table that was set to 200m.

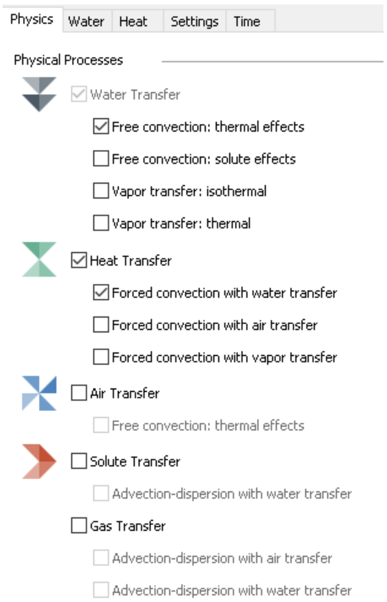

Figure 3. Physics tab for the analysis.

Given that the heat transfer option was also activated, the initial temperature profile was also required for the transient analysis, so a spatial function was defined (Table 1). For the analysis of a problem like this, there needs to be a small perturbation (disturbance) in the temperature distribution at the beginning of the analysis. This is required to get the transient numerical solution moving. It is difficult to get the solution moving in the right direction if the solutions to all equations in the domain represent perfectly uniform static conditions.

Table 1. Temperature spatial function created for the initial temperature profile.

	X (m)	Y (m)	T (°C)
Top	0	200	20.1
	200	200	19.9
	400	200	20.1
	600	200	19.9
	800	200	20.1
Bottom	0	0	26.1
	200	0	25.9
	400	0	26.1
	600	0	25.9
	800	0	26.1

The initial temperature variations along the top and bottom of the domain are hardly perceptible, but are sufficient to help with starting the free convection. The specified temperature variations along the bottom of the domain are not required to initiate the free convection. Specifying the variation at the bottom, however, speeds up the convergence process and migration towards the final steady-state conditions.

A water density function was also required in the Water tab for this analysis to define the density of the water with changing temperature (Figure 4). This density function was created using the internal algorithms of GeoStudio with the Thiesen Formula and a minimum temperature of 0°C and a maximum temperature of 40°C.

A zero pressure head boundary condition was set to the surface of the domain to ensure that the domain remains saturated for the entire simulation. The temperature along this surface was also set to 20°C using a constant thermal boundary condition. The constant thermal boundary condition along the bottom of the domain was set to 26°C to coincide with the conditions defined in Yang et al. (2010). For the temperatures used by Yang et al. (2010), of 20°C and 26°C, the water densities will be approximately 998.21 kg/m^3 and 996.77 kg/m^3, respectively, based on the function in Figure 4. This creates a density difference across the domain of 1.44 kg/m^3.

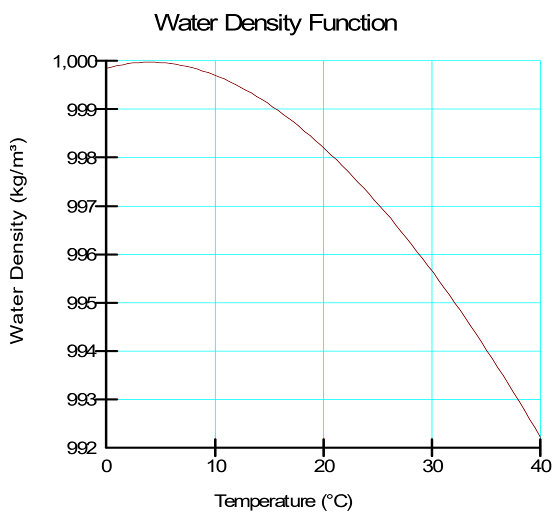

Figure 4. Water density versus temperature function used by SEEP/W.

The Simplified Thermal model was used for the thermal material model. The mass specific heat of water is defined as 4174 J/kg/°C (c_s) and the mass specific heat of the soil grains is defined as 800 J/kg/°C (c_s). This results in a volumetric specific heat of the soil-water matrix (C_m) equal to:

$$C_m = c_m \rho_m = c_w \rho_w \theta + c_s \rho_s (1 - \theta) = 2311 kJ/m^3/°C$$ **Equation 4**

The dynamic viscosity is equal to approximately 1.787x10^{-3} kg/m/s, or 1.0x10^{-3} kg/m/s for water at 20°C. The 1.787x10^{-3} value is, however, the one given in the paper and, therefore, the one used here (it is actually printed as 1.787 kg/m/s which must be a typo error). The reference density of water (ρ_w) is taken as 1000 kg/m^3. The density of the sand grains (ρ_s) is defined as 2630 kg/m^3.

The thermal conductivity of the sand grains (K_s) is reported as 2.0 W/m/°C = 2.0 J/s/m/°C and the thermal conductivity of water (K_w) as 5.0 W/m/C = 5.0 J/s/m/C. Thermal conductivity for the soil-water matrix then is calculated as:

$$K_t = K_w^{\theta} \times K_s^{(1-\theta)} = 5^{0.1} 2^{(1-0.1)} = 2.18\, J/s/m/°C$$ **Equation 5**

The porosity is reported as θ = 0.10. This value does not enter into the GeoStudio calculations even though it is specified, as the saturated only material model is used. It is used only in the hand-calculations to determine the specific heat capacity and the thermal conductivity for the soil-water matrix.

With NRA at 67, the intrinsic permeability is estimated to be $2.2x10^{-11}$ m^2. The saturated hydraulic conductivity is then computed as:

$$K_w = \frac{\rho_0 g k}{\mu_w} = \frac{1000 \times 9.801 \times 2.2 \times 10^{-11}}{1.787 \times 10^{-3}} = 1.2 \times 10^{-4} m/sec$$ **Equation 6**

To maintain numerical stability, it is necessary to slowly move the process along in incremental time steps toward the ultimate steady-state condition. The time stepping is generally controlled by what is known as the Courant number (N_{CR}). It is defined as:

$$N_{CR} = q\frac{\Delta t}{\Delta x}$$ **Equation 7**

where q is the specific discharge ($m^3/s/m^2$ or Darcian velocity, m/s), Δt is the time step size and Δx is a length interval (m). In a finite element analysis, Δx is usually the element size. In this case, the elements are 10x10 m.

Typically, the desire is to select Δt so that N_{CR} is <= 1. Physically, this means that a droplet of water moving along should not jump over too many elements. Ideally, such a droplet should move from element to element along its path.

Yang et al. (2010) report a maximum q of $5.45x10^{-7}$ $m^3/s/m^2$ (or m/s). This being the case, Δt should be around:

$$\Delta t = \frac{10}{5.45x10^{-7}} = 1.8x10^{7}\text{sec} = 212\ days$$ **Equation 8**

This gives an order of magnitude for Δt. Numerical experimentation revealed here that a Δt of 365 days (1 year) provides satisfactory results. With this as a guide, a time stepping sequence of 200 one-year time increments are used here making the total elapsed time of 200 years.

Results and Discussion

Figure 5 and Figure 6 show the resulting temperature contours and flow vectors for the simulation after 200 years. The red vectors represent the heat flow and the blue vectors represent the water flow (the vectors are displayed at different maximum lengths so that they are both visible; if they are not different then they fall on top of each other). The pattern and distribution is identical to that presented by Yang et al. (2010) as shown in Figure 1. There are also four convection cells, the same as determined by Yang et al. (2010).

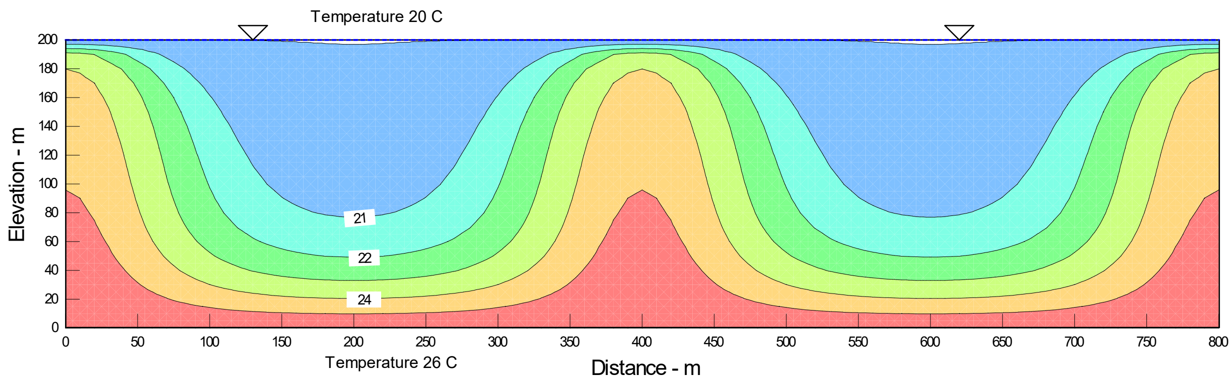

Figure 5. Resulting temperature contours for perfectly flat ground case.

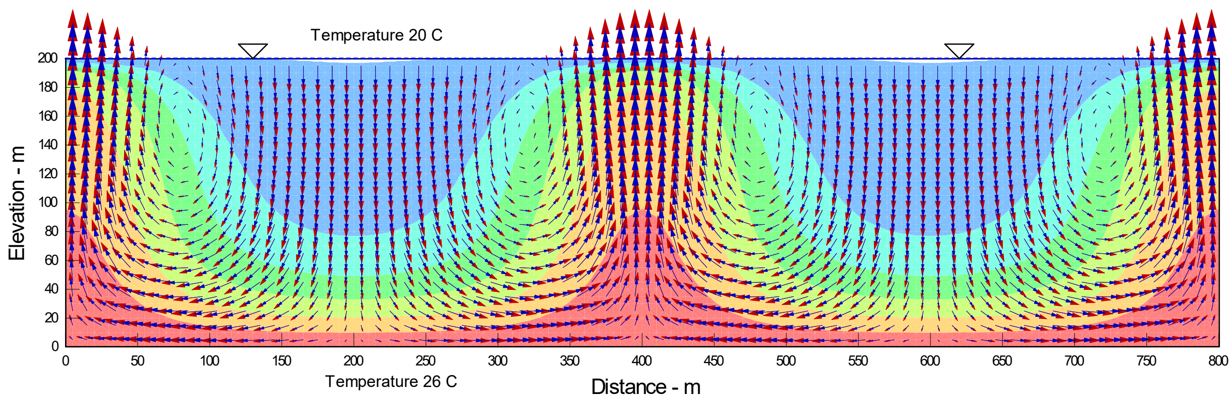

Figure 6. Convection cells and flow vectors for perfectly flat ground; red vectors represent the heat flow and blue vectors represent the water flow.

The purpose here is not to replicate all aspects of the Yang et al. (2010) study. However, looking at one case with a sloping ground surface is rather interesting. Raising the top left corner by just 0.1 m (100 mm) has quite a dramatic effect on the flow patterns. Figure 7 shows the situation at the end of 200 years. This is not the ultimate steady-state condition, but it does show the dramatic effect the gravitational (topographical) flow has on the free convection. The GeoStudio data file for this analysis is not included; it can be created by simply modifying the y-coordinate of the top left corner.

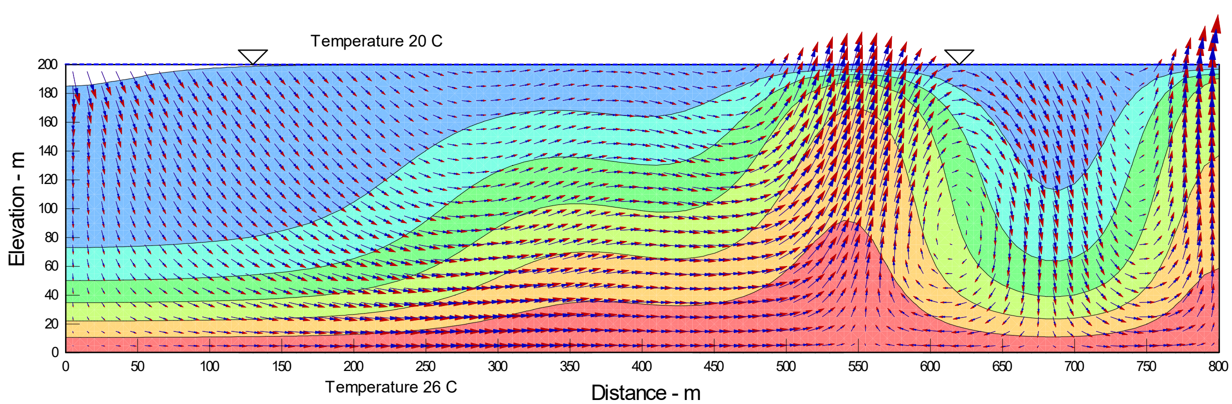

Figure 7. Flow pattern after 200 years when the left corner elevation is raised 0.1 m.

Summary and Conclusions

This analysis and the information presented here demonstrate that GeoStudio has the capability to model free convection cells in a groundwater aquifer. The results obtained match the ones computed and published independently by Yang et al. (2010).

When modeling free convection, it is important to recognize that this process only happens under special conditions. A ratio known as the Rayleigh number of the buoyance force relative to the diffusive forces needs to be within a relatively narrow range – typically between 50 and 100. Also, the flux rates in this type of process are usually rather low, which sometimes necessitates large time increments in moving the process along towards steady-state conditions. All of this requires careful consideration of the input parameters prior to running the analysis.

References

Holzbecher, Ekkehard. 1998. Modeling Density-Driven Flow in Porous Media. Springer-Verlag Berlin.

Lapwood, E. R. 1948. Convection of a fluid in a porous medium. Cambridge Phil. Soc. Proc., v. 44, p. 508-521.

Yang J W, Feng Z H, Luo X R and Chen Y R (2010). Numerically Quantifying the Relative Importance of Topography and Buoyancy in Driving Groundwater Flow, Science China-Earth Sciences, Vol. 53, No. 1, pp 64-71